CROATICA CHEMICA ACTA
CCACAA, ISSN 0011-1643, e-ISSN 1334-417X
Croat. Chem. Acta **83** (2) (2010) 113–120.
CCA-3400

Preliminary Communication

Photoelectrochemical Study of Anodically Formed Oxide Films on Niobium Surfaces

Irena Mickova

Faculty of Technology and Metallurgy, Ss. Cyril and Methodius University in Skopje, Ruger Boskovic 16, 1000 Skopje, Republic of Macedonia
E-mail: mickova@tmf.ukim.edu.mk

RECEIVED JULY 8, 2009; REVISED NOVEMBER 2, 2009; ACCEPTED DECEMBER 4, 2009

Abstract. The semi-conducting properties of electrochemically formed oxide films onto Nb surface in 1 M H_2SO_4 have been studied by photo-electrochemical measurements. By cyclic voltammetry the *I vs. E* profile of active/passive transition of Nb electrode has been recorded in the potential region from –0.5 to 8 V (SCE). The photocurrent maximums, band gap energies and flat potentials of anodic oxide films formed by stepwise rising of anodic voltage from 10 to 100 V on Nb electrode have been determined. Using Raman spectroscopy the development of crystalline structure in the films with different resultant thickness has been analysed. The semi-conducting properties of niobium oxides with development of crystalline structure have been discussed in term of breakdown processes in the films. The thresholds of transition from amorphous to crystalline form of anodic oxide films depending of applied voltages and time of polarization have been determined.

Keywords: Nb anodic films, photocurrent spectra, Raman spectroscopy

INTRODUCTION

It is well known that the passive films thicker than several nm formed on valve metal electrodes show semi-conducting properties. In the case of Nb, the semi-conducting properties of anodic oxide films can be changed in wide range by varying theirs thicknesses. The anodic oxide films always contain a deficit of oxygen which leads to the formation of oxygen vacancies.[1] The oxygen vacancies represent stoichiometric defects and act as electron donors causing the anodic oxide to be a n-type impurity semiconductor. When a Nb electrode with native oxide film formed in air is immersed in electrolytic solution, the semi-conducting-liquid junction will be established and interfacial charge transfer occurs across this junction until equilibrium is reached. The rate of charge transfer reaction in the passive films is determined by semi-conducting properties of the film. In equilibrium the Fermi level reaches the value of the electrochemical potential of the electrolytic solution and future net flow of charge transfer is stopped. The depth of the semi-conducting oxide film where the electrons are removed is denoted depletion width or depletion layer. The depletion width will depends from the initial difference of the electrochemical potential between semi-conducting and liquid phase, *i.e.* nature of metal oxide, type and concentration of electrolyte. The charge transfer reactions will caused bands bending of semi-conducting and valence bands in the depletion layer of the film. This bands bending is specific property for each semiconductor-liquid junction *i.e.* physical properties of the investigated oxide films. The oxide films onto Nb electrode can easily be thickened with well controlled thickness by anodic oxidation.[2]

The electrochemically formed anodic oxide films on Nb surfaces with approximately chemical composition of Nb_2O_5 have been of great interest for enhancing the resistant against corrosion,[3] production of electrolytic capacitors,[4] display devices based on electrochromic effects,[5] humidity sensors[6] *etc.* For this reason Nb and its oxides have been subjected to intensive investigations concerning the anodic oxide films formation in various electrolytes,[7] kinetic of oxide film growth,[8] stability and corrosion resistance of Nb covered with anodic oxide films in various aggressive media,[9] optical and semi-conducting properties of anodic oxide films with various thicknesses[10,11] *etc.* For all these investigations various measurements techniques have been used: (i) ellipsometry for determination of kinetic laws of film thickness growth and refractive indices of anodic oxide

films,[12] (ii) electrochemical characterization of anodic oxide films by cyclic voltammetry current-potential profiles and impedance spectra,[7,13] (iii) electron microscope observation the crystallization,[14] (iv) XPS spectra for hydrogen adsorption during the anodic polarization,[15] (v) ESCA spectra for investigation of chemical composition of anodic oxide films,[16] (vi) reflectance spectra and reflectivity measurements for studies of electro-chromic effects and interference films,[17] (vii) capacitance measurements for determination of semiconducting properties.[18,19] Concerning the semiconducting properties of Nb oxide films, most of studies have been concentrated to the initial stage of electrochemically formed oxde films, using EIS and capacitance measurements.[20,21] But in the study of anodic oxide films, *in-situ* photo-electrochemical techniques are particularly convenient because these films could efficiently absorb the incident light during illumination, creating delocalized charges. In contact with electrolyte solutions the delocalized charges will produce electrical current whose intensity will present photocurrent spectra for various wavelength of illumination. The thin electrochemically formed oxide films of Nb is less studied with photocurrent spectra than with EIS and capacitance measurements.[22,23] The thicker anodic oxide films have not been also enough studied with photoelectrochemical techniques, especially not in relation with development of crystalline structure in the films and breakdown processes.

In this work the photo-electrochemical properties of semi-conducting oxide films formed at constant potentials/voltages and time of anodization onto Nb in 1 M H_2SO_4 with different resultant thickness have been studied. The developments of crystalline structure with film thickness growth have been analysed with Raman spectroscopy. The transition of amorphous to crystalline Nb_2O_5 films have been discussed with initial breakdown processes in the films.

EXPERIMENTAL

Electrodes

The working electrodes were prepared from commercial pure 99.8 % niobium rod (Alfa Aesar, JMC USA). Nb rod was cut from an annealed sheat in the form of discs 6.35 mm in diameter and height of 2 – 3 mm. Before anodic oxidation one side of each disc was successively abraded with various grade silicon carbide papers up to grain size of 5000 μm. After washing and ultrasonic cleaning the discs were mirror polished with diamond sprays until grain size to 0.1 μm. Again washing in stream of water and ultrasonic cleaning in ethanol was necessary to remove all traces from diamond sprays. The last step is dried of discs in stream of compresed air and placed in teflon holder. The polished side of the discs in the teflon holder have been in contact with electrolytic solution in the photo-electrochemical cell.

Photo-electrochemical Cell

A classical three comportment electrochemical cell was built from quartz and adopted for simultaneous in-situ electrochemical, photo-electrochemical and Raman spectroscopy measurements. The working electrode together with teflon holder was fixed in the photo-electrochemical cell. As a counter electrode in the cell was placed a Pt grill with large surface and as a reference electrode the saturated calomel electrode was used. Prior to each experiment the electrolytic solution in the cell was purged with N_2.

Solutions

All experiments were carried out in 1 M H_2SO_4. This solution was prepared from 96 % H_2SO_4 (*p.a.*) (Merck) and triply distilled water. After each measurement the solution in the cell was echanged in order to avoid a soluble build-up of Nb species.

Anodic Oxidation

The anodic oxidation of Nb in the potential range from –0.5 to 8 V SCE was performed by cyclic voltammetry using HEKA (model 488) potentiostat/galvanostat, interfaced with PC. For voltages higher than 10 V the two electrode system (working and counter electrode) was used.

Apparatus and Measuring Procedure

The photocurrent measurements were carried out with experimental set-up consisting of: photoelectrochemical cell, potentiostat/galvanostat (Heka model 488) interfaced with PC, xenon lamp (500 W) coupled with monochromator (McPherson GM252), choper (EG&G model 125 A), two phase lock-in amplifier (PAR 2308) and register. The block diagram of this set-up is described elsewhere.[24] On already formed anodic oxide film, a small anodic potential was applied to the working electrode in order the constant current to flow through the photoelectrochemical cell. By illumination of semi-conducting working electrode, with energy greater or equal of the band gap energy, the excess of electron-hole pairs will be generated. The migration of these charge carriers produces a photo current.

For determining of flat-band potential the used experimental set-up consisted: pulsed excimer laser for the excitation of photocurrent (EL Lambda Physik, EMG 101) at wavelength of 308 nm, pulls duration of 20 ns and intensity up to 35 mJ/cm^2, potentiostat/galvanostat and digital storage oscilloscope (DCO,

Tektronix 7603) interfaced with PC. The block diagram of this set-up is described elsewhere.[24] The working electrode with previously formed anodic oxide films was positioned in electrochemical cell to light beam in order to obtain maximum photocurrent response during the illumination. For obtaining the maximum sensitivity of the measurements, the wavelenght of the incident light has been chosen close to the apparition of the photocurrent peaks. By potentiostatically polarisation of working electrode the pulsed laser illumination will excitant charge carriers and generate the photocurrent. Each laser pulse causes an anodic current registered on the oscilloscope. The integrated and averaged photocurrent pulses have been plotted on PC. For determination the flat-band potential the applied potential to the working electrode was step-wise adjusted to anodic or cathodic direction to obtain $I_{ph} = 0$, *i.e.* straight light position of the current pulses on the oscilloscope. The applied potential which correspond to $I_{ph} = 0$ represent the flat band potential.

The Raman spectra of native and anodic oxide films were recorded with a "Reinshaw Ramanscope" using a red laser (633 nm) illumination at a power of 1 mW.

RESULTS AND DISCUSSION

Cyclic Voltammetry Data

In Figure 1, a cyclic voltamogram of Nb electrode recorded in 1 M H_2SO_4 solution obtained for the potential region from −0.5 to 8 V (SCE) is shown.

In the first positive potential scan a well defined anodic current peak A located at about 0.1 V (SCE), that belong to the active dissolution of the metal, is observed. As suggested in Ref. 25, metal dissolution occurs via reaction

$$Nb \rightarrow Nb^{5+} + 5e^- \quad (1)$$

For more positive potentials than peak A, during the scan the anodic current decrease towards a low values corresponding to the beginning of the electrochemical passivation of the electrode following the reaction

$$2Nb + 5H_2O \rightarrow Nb_2O_5 + 10H^+ + 10e^- \quad (2)$$

The thickness of the passive film grows by reaction (2) and the metal dissolution is hindered. In the passive region that belongs to the current plateau, Figure 1, when the electrode potential reaches a value near the 2.2 V, two small anodic peaks begins to appear. It seems that the origin of these two small peaks B and C in the passive region is still unclear. So far in literature data can find various explications as: oxygen evolution,[26] consequence oxidation of the passive layer with change in the chemical composition and the ratio of existing Nb oxides in the passive film,[27] accumulation of oxygen vacancies,[28] *etc*. But our systematic measurements have shown that the shape of the cyclic voltamograms and intensity of these anodic peaks strongly depend from: pH of the electrolytic solutions, surface preparation of electrode surface (mechanical polishing, chemical polishing or electrochemical polishing) and also from cathodic pre-treatment of Nb electrode before the potential scan.[13,27] For example, in stronger H_2SO_4 and KOH solutions (2 − 10 M), for faster scan rate ($v = 50 - 200$ mV/s), the anodic peak B and C for mechanically polished Nb surface with emery paper of grain size 600 μm are more intensive and quite higher than the peak A. The peaks B and C drastically decrease in intensity for fine mechanical polished Nb surface with diamond spray, grain size down to 0.5μm (Figure 1), while for electropolished Nb surfaces these two peaks completely disappears and the passive region is flat with already constant value of current density until 8 V (SCE).

As when cyclic voltammetry scan is reversed, the

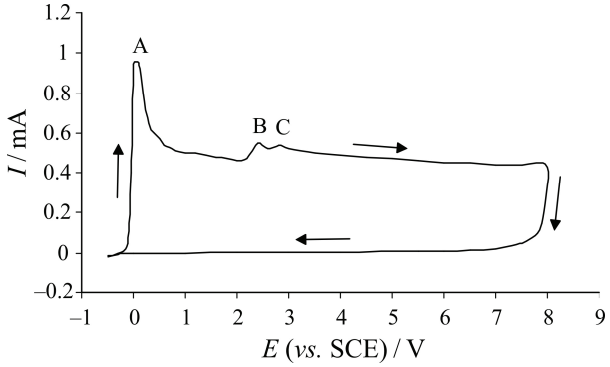

Figure 1. Cyclic voltamogram of Nb electrode recorded in 1 M H_2SO_4 between −0.5 and 8 V (*E vs.* SCE), (scan rate, $v = 0.5$ V/s).

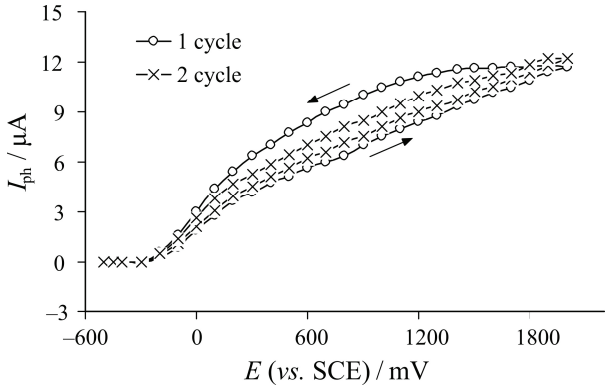

Figure 2. Dependence of photocurrent with applied potential in the passive region on Nb electrode. The measurements were carried out in 1 M H_2SO_4, (scan rate, $v = 2$ mV/s).

current decrease sharply followed by large current plateau with values close to zero up to −0.4 V (SCE). On the cyclic voltamogram no cathodic current contributions corresponding to the electro-reduction of surface oxides are observed. The tendency of Nb to form stable oxides strongly suggested that, during the first positive scan the irreversible processes occur at the electrode surface involving some niobium sub-oxides.[29]

Photo-electrochemical Data

According to Figure 1, the electrochemically formed passive film belongs to the current plateau in the potential range approximately from 0.5 V to 8 V. By stepwise increasing the anodic potential in the passive region increase the thickness of the passive film onto Nb electrode. The thickness of the film also grows with time of anodization at fixed anodic potentials.

In Figure 2, the potential dependences of the photocurrent measured in the passive region from −500 to 2000 mV (SCE) are given. The measurements were carried out at wavelength of 308 nm, where, according to Figure 3, the measured photocurrent exhibit approximately maximum values.

First cycle represents the variation of photocurrent with potential during the electrochemical passive film formation on a fresh Nb electrode. In the first positive scan from starting potential of −500 mV (the value near the steady state potential of Nb in 1 M H_2SO_4) to 2000 mV the photocurrent grows already linearly reaching a maximal value of 11.7 μA. Upon reaching the potential of 2000 mV, the scan was reversed. On the reverse scan the $I_{ph}-E$ curve decrease with potential reaching the value of $I_{ph}=0$ μA at −300 mV (SCE). At more cathodic potentials than −300 mV, not inversion in the sign of the photocurrent was observed. In the second forward and reverse scan, the photocurrent curves have closer values to each other than in the first forward and reverse scan, indicating that the already formed passive film in the first scan is stable without changes of film thickness, chemical composition and conductivity. The similar behaviour is also monitored in the next cycles. After the first cycle the film thickness is virtually independent of applied potential. The recorded photocurrent in the passive region during the cyclic voltammetry film thickness growth is in relatively good agreement with values of photocurrent given from S. Piazza et all.[25] The small difference in the shape between our and their $I_{ph}-E$ curves is caused from difference of used wavelength of illuminated light source, $\lambda=308$ nm from our side and $\lambda=260$ nm from their side.

On Figure 3, the photocurrent spectra of anodic oxide films formed at 5 V (SCE) are shown. For a longer polarization time at a constant applied anodic potential of 5 V (SCE) increase the film thickness and the strength of the electrical field in the film is diminished.

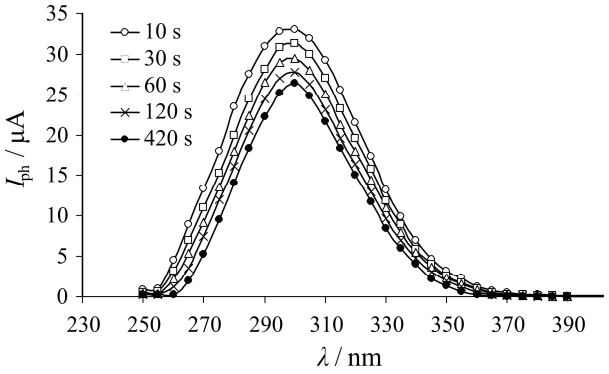

Figure 3. Photocurrent spectra, corrected for the lamp efficiency, of anodically formed films for various time of polarization on Nb electrode at 5 V (SCE) in 1 M H_2SO_4.

This provoked less density of generated charge carriers and less bending of bands during the illumination that leads to the diminution of photocurrent. The diminution of photocurrent maxima with increasing the film thickness could be explained by change of absorption coefficient. The absorption coefficient α depends on the photon energy in the following manner

$$(\alpha h\nu)^{1/2} = B(h\nu - E_{bg}) \quad (3)$$

α – absorption coefficient
B – constant that depends of investigated semiconductor
$h\nu$ – photon energy
E_{bg} – minimum energy for band gap transition

By using the relationship[30]

$$(i_{ph}\, h\nu)^{1/2} = B(E_{bg} - h\nu) \quad (4)$$

it can assume proportionality between i_{ph} and α.

From data of photocurrent spectra on Figure 3 the band gap energy of electrochemically formed oxide

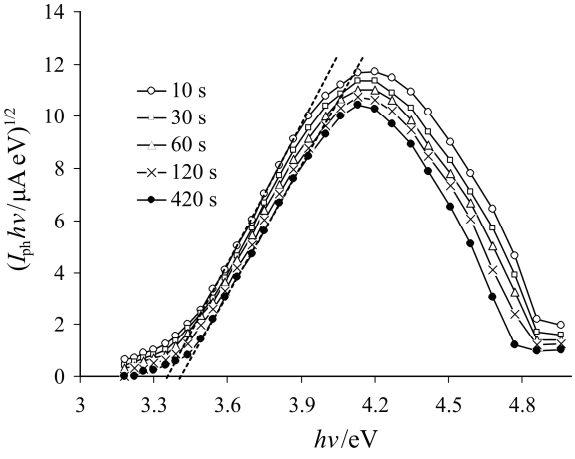

Figure 4. Determination of optical band gap energies from spectra on Figure 3.

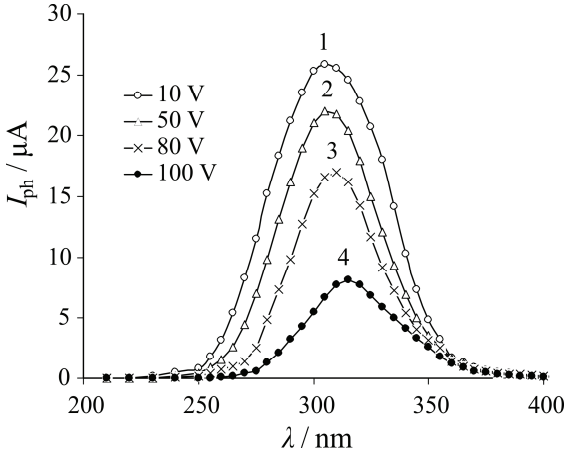

Figure 5. Photocurrent spectra corrected for the lamp efficiency, of anodically formed films during polarisation of 30 s on Nb electrode for various voltages in 1 M H_2SO_4.

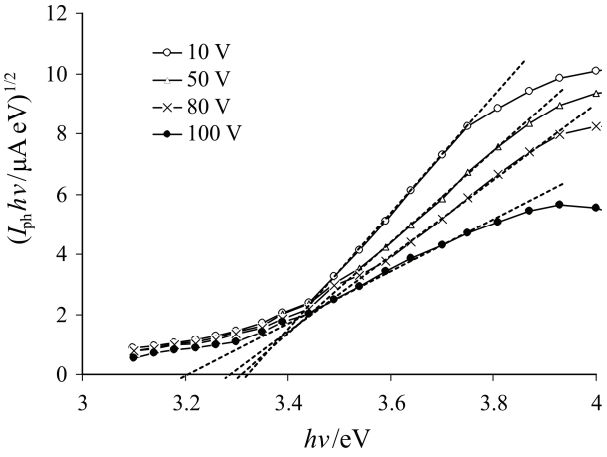

Figure 6. Determination of optical band gap energies from spectra on Figure 5.

films for various time of anodization could be determined. For these determinations the measured photocurrent from Figure 3 should be graphically presented as $(I_{ph}\,h\nu)^{1/2}$ *vs.* $h\nu$ plots.

By the abscise axis intercept of the linear plots from Figure 4, the band gap energies could be determined. As it can see from Figure 4 the band gap energy for all investigated time of anodization is almost the same with value about $E_{bg} = 3.33 - 3.38$ eV and already independent to the small variation of the film thickness.

On Figure 5, the photocurrent spectra of thicker anodic oxide films formed at various voltages during polarisation of 30 s are shown.

Similarly as in Figure 3, with increasing of film thickness the measured photocurrent decreases, *i.e.* at higher voltages of anodization the intensity of photocurrent weakened. This diminutions and shifts of photocurrent maxima to the higher wave number are the result of stepwise increasing the film thickness and beginning of film breakdown.

From photocurrent spectra on Figure 5, by replotting the photocurrent values as $(I_{ph}\,h\nu)^{1/2}$ *vs.* hν the band gap energies can determine. With extrapolation of linear portion of each curve to the x-axis, similar as in Figure 4, the band gap energies in the energy region from 3.2 eV to 3.31 eV have been determined, Figure 6.

At higher voltage anodization, as a result more intensive film breakdown raise the film inhomogeneity and the thicker films exhibit the smaller band gap energies indicating augmentation of film conductivity.

In literature can find various definition and terminologies for breakdown processes as: breakdown voltage, electrical breakdown voltage, electrolytic breakdown, dielectric breakdown, cathodic breakdown *etc.*[31–33] In all these cited types of breakdown are taken in consideration that during the anodic polarization there is the limit to the thickness beyond which the film breaks down. The breakdown for a same metal electrode covered with oxide film can have various values depending of: film thickness, type and concentration of electrolyte used, anion insertion from electrolyte solution into the film, pre-treatment of electrode surface etc. The voltage at which the anodic oxide film reaches the critical thickness at begins to break is known as electrical breakdown voltage. It was defined as voltage at which visible sparking was observed to start or, in the absence of sparking, the steady voltage that was achieved at constant current.[33] The sparks associated with a strong electrical field that extended into the solution and involve injection of anions into the film is known as electrolytic breakdown. Except of breakdown, the crystallization is also associated with film thickness. Draper and Harvey studied crystallization on anodic films on tantalum and niobium under breakdown voltage.[34] They were also noted that some crystallization accompanied breakdown. In reality, the breakdown process begins at very lower voltages that before apparition of visible spark. The initial breakdown process can recorded oscilloscopically as oscillations of steady state currents at constant voltage. For example, the first initial breakdown process on Ti electrode in 0.1 M Na_2SO_4 is observed at 5 V and the second at 65 V.[31] The first breakdown correspond to beginning the transition from amorphous to micro-crystalline structure and second form micro-crystalline to well crystallized anatase structure.

Concerning the Nb electrode, the change of photocurrent spectra with film thickness is also related with transition from amorphous to crystalline structure. In the voltage region between 10 and 100 V the initial breakdown without visible spark has been recorded at about 15 V. The base colour of Nb film formed at this voltage is violet, but in the metallographic image the small number of yellow grains, that correspond to lower formation voltage, sheared among big number of violet grains have been observed. The apparition of yellow

Table 1. Characteristic semiconducting parameters on Nb anodic oxide films, obtained during the photocurrent measurements

Voltage	$I_{ph(max)}$	λ_{max}	E_{bg}	E_{fb}
V	μA	nm	eV	mV
5	31.30	300	3.34	−445
10	25.91	305	3.31	−450
50	22.00	307	3.30	−470
80	17.00	310	3.27	−500
100	8.10	315	3.20	−660

grains indicated beginning the destruction of film, *i.e.* initial breakdown process and initial development of film inhomogeneity. However with increasing the anodization voltage until 100 V, increase the number of structural defects in the film, so that during the more intensive breakdown in the structure of anodic oxide films it is also possible inclusions of electrolyte anions, that would significantly influenced to the semiconducting properties of the film.

In Table 1 are listed the values of photocurrent peaks with corresponding wavelength, band gap energies and flat band potentials (potentials at zero electrical field in the film) measured for each investigated thickness of anodic oxide films.

The flat band potential mainly depends from the: film thickness, pH of the electrolytic solution, structural defects in the film *etc*. All these parameters influenced to the value of electrical field in the depletion layer of anodic oxide films. It was shown that a big difference in the strength of electrical filed into amorphous and crystalline films exist.[35] In the thinner oxide films formed by a field assisted growth process when strength of the built up electrical field reach the value up to 10^5 V/cm, the migration of photo-generated charge carriers decrease to very low value, essentially due to the effect of the long-range disorder in amorphous structure.[26] With increasing the film thickness the average concentration of donors becomes smaller also as a consequence of the higher defect concentration in the film. The breakdown process and values of flat band potentials are in close relation with crystallisation of the anodic oxide films. As it can se from Table 1, with film thickness growth the flat band potential is shifted to cathodic direction. Schultze and Lorhengel proposed that on valve metal electrodes the electrochemically formed oxide films in the passive potential region are amorphous. But with increasing the applied anodic voltage develop crystallisation in the films, followed with more intensive breakdown processes.[36] In this work the development of film crystallinity was studied with Raman spectroscopy.

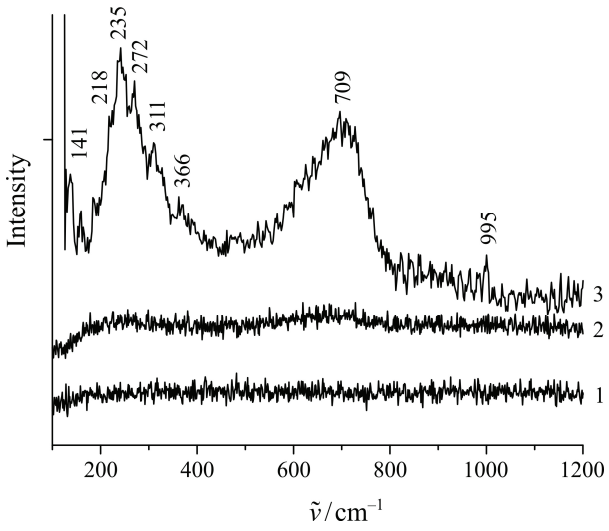

Figure 7. Raman spectra of Nb electrodes anodically polarized in 1 M H_2SO_4 for various voltages: open circuit potential (1), 10 V (2), 50 V (3).

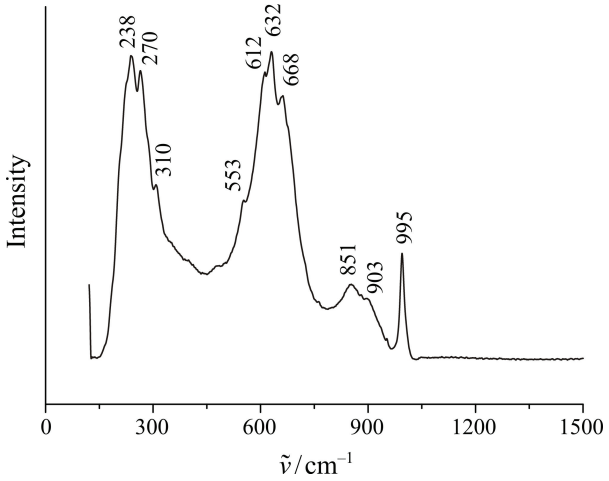

Figure 8. Raman spectrum of Nb electrode anodically polarized at 100 V in 1 M H_2SO_4.

Raman Spectroscopy Data.

Raman spectroscopy is very sensitive to the structure and band order of metal oxides, especially in the region of metal-oxygen stretching modes. The long and short range lattice disorder influenced significantly on the electronic properties of amorphous semiconducting films. For thin anodic oxide films formed in the passive potential region (cyclic voltamogram Figure 1), no active Raman bands were monitored, indicating amorphous structure of these films Figure 7.

According to literature data, these films exhibit more complex structure that anodic oxide films and they are consisted from mixture of: NbO_2, Nb_2O_5 and Nb_2O_5 nH_2O.[37,38] During the potential scan of Nb electrode, in

the passive potential region NbO_2 is irreversibly oxidised to Nb_2O_5. With stepwise increasing the anodic potential, the first noticeable broad and ill defined Raman bands, approximately located on 235 cm^{-1} and 700 cm^{-1} appear at 10 V, indicating beginning the structural order in the film. Continuing the augmentation of anodic voltage these two Raman bands rise in intensity and new additional bands begin to appear. On anodic voltage of 50 V, (Figure 7, curve 3), the band at 709 cm^{-1} become stronger, less broad and relatively well defined, while the broad band at 235 cm^{-1} become also stronger and coupled with many other medium and weak bands characteristic for NbO_2 and Nb_2O_5 structures. The raising of existing and apparitions of new additional bands is characteristic for transition from amorphous to crystalline structure and development of crystallisation. At 50 V the film is composed of short range micro-crystallites. The band located at 709 cm^{-1} is the key band of NbO_2 while the band centred at 235 cm^{-1} is characteristic for Nb_2O_5. The spectra in Figure 7, correspond to transformation of amorphous to micro-crystalline and development of micro-crystallites in the oxide film.

At anodic voltage of 100 V, the key band of NbO_2 at 709 cm^{-1} disappears and new strong band at 650 cm^{-1}, coupled with additional medium (at 632 cm^{-1}) and weak bands (at 612 and 668 cm^{-1}) characteristic for Nb_2O_5 are registered, Figure 8.

All registered Raman bands bellow 200 cm^{-1} are due to external modes. These bands also show some systematic with a band around being common to all the oxides and could be assigned to a metal-metal vibration mode[39]. The Raman band at 235 cm^{-1} become from the bending mode of Nb–O–Nb. The bands in the 400–800 cm^{-1} wavenumber region are assigned to the symmetric and anti symmetric stretching mode of the Nb–O–Nb linkage. The Raman bands at 650 cm^{-1} are intense and often appear as doublets or triplet due to the Nb_2O_5 anisotropy. The Raman bands located in the high wavenumber region 850–1000 cm^{-1} are characteristic of the symmetric stretching mode of Nb=O terminal double bond. The band at located at 996 cm^{-1} correspond to the metal-oxygen stretching vibration in Nb_2O_5, which can shift to either the high or low frequency side, due to different structural distortions. The spectra in Figure 8, correspond to well developed crystalline structure of Nb_2O_5.

CONCLUSION

From cyclic voltammetry, photo-electrochemical and Raman spectroscopy measurements of anodic oxide films formed on Nb surfaces in 1 M H_2SO_4, the following conclusions can be drawn.

The $I–E$ profile of cyclic voltamogram of Nb electrode exhibits one well defined anodic current peak A followed by a wide passive potential region, typically for valve metal electrodes of Nb and Ta. In the passive potential region, between 2.2 and 3 V, additional small anodic peaks B and C appear. The origin of these two small peaks can be attributed to: consequent oxidation of Nb oxides in the passive films, evolution of oxygen or accumulation of oxygen vacancies. Our investigations have shown that the intensity of these two peaks strongly depends for surface pre-treatment of Nb electrode and that on the cyclic voltamogram of electropolished Nb surface these two peaks do not exist.

In passive potential region, during the film formation from -0.5 V to 2 V, the photocurrent rise in intensity with applied anodic potential. After the film formation in the first forward cycle, the film exhibit almost constant thickness and with consequent cyclisations the shapes of $I_{ph}-E$ curves are almost unchangeable. The formed film is relatively stable and the variation of photo-current during the cyclisation is a result of smaller or bigger generation of charge carriers.

For anodic oxidation at 5 V, the small decrease of photo-current maxima with time of anodization is due to the change of film thickness. The film thickness grows influenced to the diminution of band gap energy from 3.38 – 3.33 eV.

With increasing of applied anodic voltage from 10 to 100 V the photo-current maxima decreases in intensity and shift toward higher wavenumber as a result of increasing the: film thickness, breakdown processes and development of crystallinity. The determined band gap energies and flat band potentials varied from 3.31 to 3.2 eV and from -450 mV to -660 mV respectively, indicating that the development structural defects and crystallinity strongly influenced to the film conductivity.

With stepwise augmentation of anodic voltage the Raman spectra have confirmed the transition of amorphous structure of the passive film to micro-crystallites and change of chemical composition of the film. The micro-crystallites are consisted from mixture of NbO_2 and Nb_2O_5. However for higher anodic voltages, from 60 V to 100 V the micro-crystallites transform to long range crystals and the NbO_2 component in the film is transformed to Nb_2O_5 well crystallized form.

Acknowledgements. The Raman spectroscopical and photocurrent measurements were performed in the "Institute fur Physikalische Chemie und Electrochemie, Technische Universitat Dresden". The author wish to thank Prof. W. Plieth and Dr. N. Hebestreit.

REFERENCES

1. K. E. Heusler and M. Schulze, *Electrochim. Acta* **20** (1975) 237–244.
2. I. Arsova, A. Prusi, Lj. Arsov, J. *Solid State Electrochem.* **7** (2003) 217–222.

3. I. Uehara, T. Sakai, H. Ishikawa, H. Takenaka, *Corrosion* **45** (1989) 548–553.
4. H. Brunner, F. Emmenegger, M. Robinson, H. Rotschi, *J. Electrochem. Soc.* **115** (1968) 1287–1289.
5. B. Ohtani, K. Iwai, S. Nishimoto, T. Inui, *J. Electrochem. Soc.* **141** (1944) 2439–2442.
6. N. Kurioka, D. Watanabe, M. Haneda, T. Shimanouchi, T. Mizushima, N. Kakauta, A. Ueno, T. Hanaoka, Y. Sugi, *Catalysis Today* **16** (1993) 495–501.
7. G. Cavigliasso, M. Esplandiu, V. Makagno, *J. Appl. Electrochem* **28** (1998) 1213–1219.
8. C. D. Alkine, L. de Souza, F. Nart, *Corros. Sci.* **34** (1993) 117–127.
9. D. Sandulov, N. Ustimenko, M. Eidelberg, *Elektrokhimiya* **24** (1988) 433–436.
10. W. Badawy, A. Fekske, W. Plieth, *Electrochim. Acta* **34** (1989) 1711–1715.
11. A. Modestov, A. Davydov, *J. Electroanal. Chem*. **460** (1999) 214–225.
12. I. Arsova, Lj. Arsov, N. Hebestreit, A. Anders, W. Plieth, *J. Solid State Electrochem.* **11** (2007) 209–214.
13. I. Mickova, A. Prusi, T. Grchev and Lj. Arsov, *Portugal Electrochim. Acta* **24** (2006) 377–385.
14. R. Pawel, J. Campbell, *J. Electrochem. Soc.* **111** (1964) 1230–1234.
15. P. Wong, Y. Li, A. Mitchell, Surf. *Rev. Lett*. **2** (1995) 495–499.
16. M. Grunder, J. Halbritter, *J. Appl. Phys.* **51** (1980) 397–405.
17. J. Juliao, J. Chages, H. Cesar, N. Dias, F. Decker, U. Gomes, *Electrochim. Acta* **36** (1991) 1297–1300.
18. F. Di Quarto, S. Piazza, C. Sunseri, *Electrochim. Acta* **35** (1990) 99–107.
19. V. Egoerov, P. Lukovtsev, *Elektrokhimiya*, **5** (1969) 387–391.
20. R. Torresi, F. Nart, *Electrochim. Acta* **33** (1988) 1015–1018.
21. C. Dyer, J. Leach, *Electrochim. Acta*, **20** (1975) 161–160.
22. S. R. Biaggio, N. Bocchi, R. C. Rocha-Filho, F. E. Varela, *J. Braz. Chem. Soc.* **8** (1997) 615–620.
23. A. I. de Sa, C. M. Rangel, P. Skeldon, G. E. Thompson, *Portugal Electrochim. Acta* **24** (2006) 305–311.
24. I. Mickova, *Maced. J. Chem. Chem. Eng* **28** (2009) 181–188.
25. S. Piazza, C. Sunseri, F. Di Quarto, *J. Electroanal. Chem.* **293** (1990) 69–84.
26. F. Di Quarto, S. Piazza, C. Sunseri, *Ber. Bunsenges. Phys. Chem.* **91** (1987) 437–441.
27. I. Mickova, A. Prusi, T. Grchev, Lj. Arsov, *Croat. Chem. Acta* **79** (2006) 527–532.
28. S. R. Morrison, *Electrochemistry of Semiconductors and Oxidized Metal Electrodes*, Plenum Press, New York 1980.
29. F. Di Quarto, S. Piazza, C. Sunseri, *J. Chem. Soc. Faraday Trans. I* **85** (1989) 3309–3313.
30. N. Mott, E. Davis, *Electronic Processes in Non-crystalline Materials*, 2nd Ed, Clarendon Press, Oxford (1979).
31. J. Yahalom, J. Zahavi, *Electrochim. Acta* **15** (1970) 1429–1435.
32. K. Kalra, K. Singh, M. Singh, *J. Electroanal. Chem.* **371** (1994) 73–78.
33. R. Alwitt, A. Vijh, *J. Electrochem. Soc.* **116** (1969) 388–390.
34. P. Draper, J. Harvey, *Acta Metall.* **11** (1963) 873–879.
35. U. Stimming, *Electrochem. Acta* **31** (1986) 415–428.
36. J. Schultze, M. Lohrengel, *Electrochm. Acta* **45** (2000) 2499–2513.
37. B. Huang, K. Wang, J. Church, Y. S. Li, *Electrochim. Acta.* **44** (1999) 2571–2577.
38. I. Arsova, A. Prusi, T. Grchev, Lj. Arsov, *J. Serb. Chem. Soc.* **71** (2006) 177–187.
39. A. McConnell, J. Anderson, C. Rao, *Spectrochim. Acta, Part A* **32** (1976) 1067–1076.

SAŽETAK

Fotoelektrokemijski studij anodno stvorenih oksidnih slojeva na površini niobija

Irena Mickova

Faculty of Technology and Metallurgy, Ss. Cyril and Methodius University in Skopje, Ruger Bošković 16, 1000 Skopje, Republic of Macedonia

Fotoelektrokemijski su mjerena poluvodička svojstva elektrokemijski stvorenih oksidnih slojeva na površini niobija u 1 M H_2SO_4. Cikličkom voltametrijom određene su ovisnosti struje o potencijalu za prijelaz aktivnog u pasivni sloj u području potencijala između −0.5 i 8 V prema ZKE. Određeni su maksimumi fotostruja, energije razmaka među vodljivim vrpcama i "flat" potencijali anodnih oksidnih slojeva stvorenih stepenastim porastom anodnog potencijala od 10 do 100 V. Razvoj kristalne strukture slojeva različitih debljina analiziran je Ramanovom spektroskopijom. Diskutirana je veza poluvodičkih svojstava niobijevog oksida sa razvojem kristalnih struktura i procesa urušavanja slojeva. Pokazano je da početak prijelaza amorfnog anodnog oksida u kristalni oblik zavisi o naponu i trajanju polarizacije.